I&EC research
Industrial & Engineering Chemistry Research

Article

Cite This: Ind. Eng. Chem. Res. 2020, 59, 52−60

pubs.acs.org/IECR

Hydrogen Partitioning as a Function of Time-on-Stream for an Unpromoted Iron-Based Fischer−Tropsch Synthesis Catalyst Applied to CO Hydrogenation

Alisha L. Davidson,[†] Paul B. Webb,*[,‡] Stewart F. Parker,[§] and David Lennon*[,†]

[†]School of Chemistry, University of Glasgow, Joseph Black Building, Glasgow G12 8QQ, U.K.

[‡]School of Chemistry, University of St Andrews, St Andrews KY16 9ST, U.K.

[§]ISIS Facility, STFC Rutherford Appleton Laboratory, Chilton, Didcot, Oxon OX11 0QX, U.K.

Supporting Information

ABSTRACT: Inelastic neutron scattering (INS) is employed to examine the evolution of a promoter-free iron-based Fischer−Tropsch synthesis catalyst (∼10 g catalyst charge) that is exposed to ambient pressure CO hydrogenation at 623 K for up to 10 days time-on-stream (T-o-S). The longer reaction time is selected to better understand how the formation of a previously described hydrocarbonaceous overlayer corresponds to the catalyst conditioning process. Although the onset of pseudo steady-state reactor performance is observed at approximately 9 h T-o-S, INS establishes that the intensity of the C−H stretching mode of the sp^3-hybridized component of the hydrocarbonaceous overlayer saturates at about 24 h T-o-S, while the corresponding intensity of the C−H stretching mode of the sp^2-hybridized component requires 100−200 h T-o-S to achieve saturation. This novel series of measurements reveal different aspects of the complex catalyst evolutionary process to be indirectly connected with catalytic turnover.

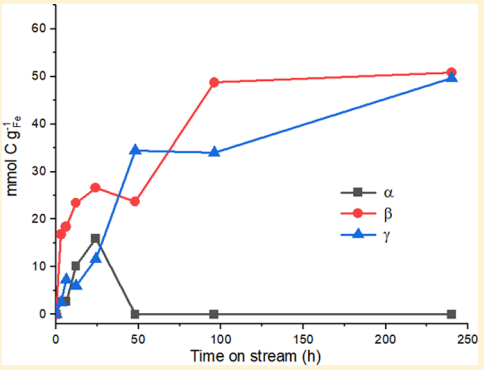

1. INTRODUCTION

Fischer−Tropsch synthesis (FTS) involves the catalytic conversion of synthesis gas, a mixture of CO and H_2, to produce a wide range of hydrocarbon products, with the synthesis gas being obtained from biomass, natural gas, or coal.[1−3] The hydrocarbon product output is dependent on not only the reaction conditions employed but also the catalyst used.[4] Current commercial processes operate with iron- and cobalt-based catalysts.[3] Iron FTS catalysts convey some favorability over cobalt catalysts on grounds of low cost and tolerance to poisons. Furthermore, through the addition of promoters or changes to reaction conditions, they are responsive to manipulation of the product slate to produce olefins and oxygenates.[3,5]

Iron-based FTS catalysts are known to go through an "evolutionary" period in the early stages of reaction. In a pretreatment step, or under FTS conditions, the oxidic precatalyst is reduced toward α-Fe and/or iron carbides.[3,5−7] The final catalyst composition and the extent of the evolutionary phase is dependent on the reaction conditions utilized.[3−5] The active phase of iron FTS catalysts is still under debate, but several studies have independently demonstrated a clear correlation between FT activity and the formation of iron carbides,[8−11] in particular, the Hägg carbide. Concerning the duration of this initial catalyst conditioning period, Pérez-Alonso et al. report that catalytic activity required a period of ca. 120 h to reach the steady state, with the changes attributed to variations in the composition of the iron catalyst in the initial stages of the reaction.[12] The duration of these changes is in general agreement with Buker and co-workers, who report an iron FTS catalyst to require approximately 100 h time-on-stream (T-o-S) to attain steady-state operation.[13] However, it is noted that the extent of the initial conditioning period will be dependent on several factors including reactor configuration, GHSV, gas consumption, pressure, and temperature. It is the iron-based FTS catalyst evolutionary phase that is the principal matter of interest in this communication.

The present study builds upon previous inelastic neutron scattering (INS) investigations of Fe-based FTS catalysts that correlate ambient pressure CO hydrogenation activity with the formation of a hydrocarbonaceous overlayer.[14−19] In particular, a recent communication by Warringham et al. examined the evolution of the hydrocarbonaceous overlayer over a reaction period of 24 h T-o-S that revealed the overlayer to be dominated by polyaromatic moieties alongside a less prominent aliphatic component.[18] With reference to sections of the selective hydrogenation literature,[20] it is further suggested that the overlayer defines the active sites on the iron carbide surface.[18] After 24 h T-o-S, the olefinic/aromatic

Received: August 21, 2019
Revised: October 23, 2019
Accepted: December 9, 2019
Published: December 9, 2019

DOI: 10.1021/acs.iecr.9b04636
Ind. Eng. Chem. Res. 2020, 59, 52−60

moiety of the overlayer continues to increase, while the population of the aliphatic feature appears to saturate after approximately 6 h.[18] If the hydrocarbonaceous overlayer does indeed play an active role in determining catalytic performance, it is opportune to consider how the nature of the overlayer is modified for reaction times beyond 24 h and to concentrate on the ∼100 h T-o-S duration, as highlighted by Pérez-Alonso and co-workers and Buker and co-workers.[12,13]

It is noted that the use of ambient pressure CO hydrogenation as a test reaction is selected for its compatibility with the INS technique.[15−18] Interestingly, the INS spectrum for the hydrocarbonaceous overlayer that forms for extended periods of T-o-S for the iron-based FTS reference catalyst examined here (CO hydrogenation, ambient pressure, 623 K, 24 h T-o-S) is remarkably similar to that of a technical catalyst that has been extracted from a large-scale commercial FTS unit operation.[18] This outcome signifies that the hydrocarbonaceous overlayer is indeed relevant to the large-scale Fe-based FT catalyst and FT process.

Given the industrial significance of iron-based FTS catalysis,[3] this article seeks to build on the work of Warringham et al.[18] and to apply the INS technique in order to discover, for ambient pressure CO hydrogenation at 623 K, how hydrogen is partitioned within an unpromoted iron FTS catalyst for extended periods of T-o-S (0−240 h). Post-reaction ex situ characterization includes elemental analysis, X-ray diffraction (XRD), Raman spectroscopy, and temperature-programmed oxidation (TPO) measurements. This combination of techniques determines how the form and nature of the overlayer is modified during the transition from a hematite precatalyst to a catalyst stabilized for CO hydrogenation activity. Collectively, this novel series of measurements over this extended reaction time reveal different aspects of the complex catalyst evolutionary process to be indirectly connected with catalytic turnover.

2. EXPERIMENTAL SECTION

2.1. Catalyst Preparation. The iron oxide sample, with no promoters or modifiers, utilized for this experiment was prepared using a co-precipitation of iron nitrate (Sigma-Aldrich, 99.99%) and sodium carbonate (Sigma-Aldrich, 99.99%), using a Mettler Toledo LabMax batch reactor apparatus to ensure reproducibility of catalyst synthesis.[18] The resulting slurry was filtered, washed with deionized water, and calcined using the same stepwise programme described elsewhere.[18] Samples were ground and sieved to a particle size range of 250−500 μm. In a separate experiment (not presented here), this material was examined for FTS activity on a semitechnical test facility operating with a syngas pressure of 25 Barg and a temperature range of 300−350 °C: The catalyst displayed sustained FTS activity for a test period duration of 6 days. It is noted that although this catalyst was prepared in exactly the same way as the catalyst examined for 0−24 h by Warringham and co-workers,[18] it is a different batch of catalyst.

2.2. INS Measurements. For INS measurements, approximately 10 g of the catalyst was loaded into an Inconel reactor cell and attached to a custom-built sample preparation apparatus.[21] As the present study concentrates on using INS to characterize the form of the hydrocarbonaceous overlayer over an extended 240 h period of reaction, only the relatively larger scale INS reactor is employed in this work. Previously, the authors have considered differences in the gas/solid exchange dynamics that can lead to retardation of reaction processes in the INS reactor compared to a more conventional microreactor arrangement.[15,17] Crucially, for this study, as all reactions are undertaken using the INS reactor, post-reaction temporal profiles using ancillary analytical methods can be directly compared to the INS spectra.

For CO hydrogenation measurements, the iron oxide catalyst samples were heated to 623 K at 5 K min^{-1} under a flow of carbon monoxide (75 mL min^{-1}, CK Gas, 99.9%) and hydrogen (150 mL min^{-1}, CK Gas, 99.9%) in a carrier gas (He, 600 mL min^{-1}, CK Gas, 99.9%, total WHSV of 1.27 h^{-1}) and held at this temperature for a predetermined length of time. It is noted that the INS measurements were not consecutive, and each time period analyzed has utilized a different charge of the catalyst. Thus, an approximately 10 g charge of the catalyst was reacted for 48 h, the reaction quenched, and the catalyst transferred to the INS spectrometer for spectral acquisition. In the case of the 96 h run, a fresh 10 g charge of the catalyst was reacted for 96 h before stopping the reaction and transferring the catalyst to the spectrometer. Likewise for the 240 h run.

The gas products were analyzed by an in-line mass spectrometer (Hiden Analytical, HPR20 QMS Sampling System). Once the reaction was complete (t = x h), the reactant gases were stopped, and the sample was left to cool to room temperature in a flow of carrier gas. The reactor cell was isolated and transferred to an argon-filled glovebox (MBraun UniLab MB-20-G, [H_2O] < 1 ppm, [O_2] < 2 ppm) before being loaded into an aluminum INS cell and sealed via an indium wire gasket for INS analysis.[22] All INS measurements were performed using the MAPS direct geometry spectrometer.[23] Spectra were recorded at 20 K at incident energies of 600 and 250 meV using the A chopper package.[23] Quantification of the ν(C−H) modes was achieved following a calibration protocol described elsewhere.[18,24] For ex situ characterization, reacted samples were subjected to a passivation procedure involving the introduction of small amounts of O_2 to the reactor, gradually increasing to atmospheric levels (i.e., 20% O_2 in the gas feed).[25] The samples prepared in the large-scale INS reactor are referred to as LR-x, where x indicates the T-o-S in hours. Three reaction times are considered: 48, 96, and 240 h T-o-S.

2.3. Post-Reaction Analysis. TPO studies of the large-scale samples were carried out ex situ on a microreactor catalyst test line. The apparatus is composed of 1/8″ diameter stainless steel Swagelok tubing; a full description of which can be found elsewhere.[17,18] Approximately, 10 mg of the catalyst was loaded into a 1/4″ quartz tube reactor with the reactor plugged with quartz wool. The reactor is housed within a tube furnace (Carbolite MTF 10/15/30) equipped with PID control and a thermocouple that is positioned within the catalyst bed to ensure accurate temperature reading during measurements. Oxygen (5% in He, 70 sccm, BOC Ltd, 99.5%) was introduced to the sample, and the reactor was heated to 1173 K at 5 K min^{-1} using the mass spectrometer to monitor the eluting gases. Quantification of the CO_2 peak area was achieved by measuring the CO_2 response from the in situ TPO of known masses of graphite (Sigma-Aldrich, 99.9%).[26] Previous ex situ TPO measurements have used larger catalyst loadings (∼40 mg), but[15−19] for the extended reaction times under consideration here that resulted in significant carbon retention; such masses caused exhaustion of the oxygen co-feed, compromising carbon quantification. TPO measurements of a lower catalyst mass of ∼10 mg ensured that the carbon

DOI: 10.1021/acs.iecr.9b04636
Ind. Eng. Chem. Res. 2020, 59, 52−60

oxidation process remained within quantitative limits for all samples examined.

Ex situ powder XRD was performed using a Panalytical X'Pert PRO MPD equipped with a Co Kα radiation. Ex situ Raman scattering was performed using a Horiba Jobin Yvon LabRam HR confocal Raman microscope and a 532 nm laser source at <20 mW power. Measurements were performed for approximately 5 min. Elemental analysis was performed on an Exeter CE-440 Elemental Analyzer (~detection limit 0.1 wt %).

3. RESULTS AND DISCUSSION

3.1. Reaction Testing Prior to INS Measurements. The catalyst under consideration here is the same as that used in the 24 h INS study undertaken by Warringham and co-workers, with XRD confirming the phase of the iron oxide sample to be hematite (α-Fe_2O_3). The sample has been additionally characterized by N_2 physisorption, XRD, Raman, scanning electron microscopy, transmission electron microscopy, and inductively coupled plasma-optical emission spectrometry that are described elsewhere.[17] CO hydrogenation at ambient pressure and elevated temperature provides information on the surface chemistry of the iron oxide/CO/H_2 reaction system without the formation of long chain hydrocarbons, which would otherwise interfere and significantly complicate the INS spectra.[14−19] Figure 1 displays

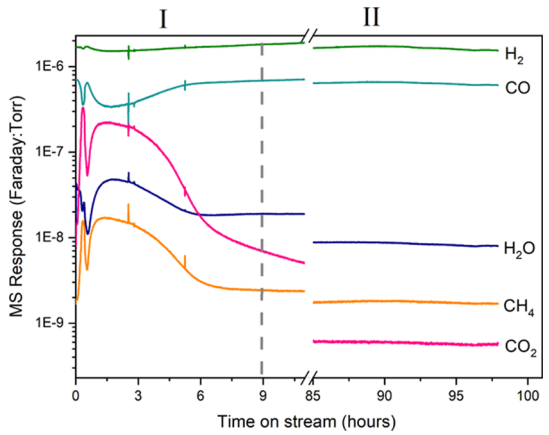

Figure 1. Reaction profile for the sample exposed to CO hydrogenation conditions at 623 K for 96 h. Roman numerals indicate different stages within the reaction profile (see the text). The vertical dashed line signifies 9 h T-o-S.

a representative mass spectrometric profile for a 0−96 h reaction and, as reported for the 24 h reaction sequence, it is divisible into two subsections:[18] (I) the simultaneous production of H_2O, CH_4, and CO_2 as the reaction reaches the temperature, followed by (II) the reaction approaching steady-state operation. The latter phase is deemed to be achieved within approximately 9 h T-o-S; thereafter, the product distribution is stable. Under these conditions, CO conversion approximates to <1%, with catalytic activity approximating to an iron time yield of 6.39×10^{-6} mmol (CO) g_{Fe}^{-1} s^{-1}, similar to values reported in the literature for bulk iron catalysts operating under similar conditions.[27] It is noted that CO_2 production drops quite dramatically over the reaction period. This was also noted by Warringham et al., who suggested the main route of CO_2 production to be predominant reduction of α-Fe_2O_3 → Fe^0.[18] With reference to Figure 1, the decrease in CO_2 correlates with the CO returning to a steady-state regime, suggesting that by approximately 9 h on stream, the catalyst is fully reduced. Figure 1 highlights the initial conditioning period and the steady-state operation at extended reaction times (0−10 and 85−100 h, respectively). Figure S1 presents an extended reaction profile that covers the range 0−100 h T-o-S.

3.2. Post-Reaction Characterization. Elemental analysis of the catalyst before and after exposure to CO hydrogenation conditions for 48, 96, and 240 h T-o-S enable the degree of carbon and hydrogen retention within the catalyst to be determined; the results are presented in Table 1. Minimal C

Table 1. Elemental Analysis of the Catalyst before and after Exposure to CO Hydrogenation Conditions for 48, 96, and 240 h T-o-S[a]

sample	wt % carbon	wt % hydrogen
α-Fe_2O_3	0.11 (±0.08)	0.08 (±0.01)
LR-48	23.42 (±0.21)	0.17 (±0.05)
LR-96	32.83 (±0.86)	0.39 (±0.14)
LR-240	34.89 (±0.66)	0.27 (±0.06)

[a]The standard deviation from measurements performed in duplicate is shown in brackets.

and H are detected in the unreacted sample. On reaction, there is a systematic trend of increasing C retention for increasing periods of T-o-S, with the C retention rate decreasing for times ≥100 h. Table 1 additionally shows hydrogen retention to be evident but to a much lesser degree than observed for C and also in a less systematic fashion. Collectively, Table 1 indicates increased retention of C (major) and H (minor) up to approximately 100 h T-o-S. Indeed, the degree of hydrogen retention is just above the detection levels of the elemental analyzer (~0.1 wt %).

Figure 2 presents the ex situ diffractograms of the catalyst pre- and post-reaction. Samples LR-48, LR-96, and LR-240 h are displayed in Figure 2b. In contrast to Figure 2a, which distinctly shows hematite (α-Fe_2O_3) reflections, Figure 2b reveals the loss of these features on reduction over the 240 h period and the emergence of various reflections in the range of 40−60°, signifying the formation of iron carbides. Rietveld refinement of the catalyst samples, details of which are presented within the Supporting Information section (Figures S2 and S3), establishes the presence of a pure Hägg carbide (Fe_5C_2) phase for the post-reaction samples. Previous work has indicated cementite (Fe_3C) to be present in the early stages of the reaction,[15] but Figure 2 is interpreted as indicating the formation of the Hägg carbide, the proposed active phase, to be completed by 48 h on stream. The broad reflections at ca. 30° are attributed to amorphous carbon; the intensity of this feature increases as T-o-S extends from 48 to 240 h.

Figure 3 presents ex situ Raman spectra of the catalyst prior to reaction (Figure 3a) and after 240 h reaction (Figure 3b). The post-reaction sample is indicative of the retention of carbonaceous species, as signified by the "D" and "G" bands that are associated with disordered and ordered graphitic carbon, respectively.[28−30] Figure 4b includes a fit to the G, D1, D3, and D4 states of carbon; consistent with the build-up of an amorphous carbon component.

Figure 4 presents the post-reaction TPO profiles. Previous measurements have identified the presence of three carbonaceous species from TPO measurements on iron-based FTS

DOI: 10.1021/acs.iecr.9b04636
Ind. Eng. Chem. Res. 2020, 59, 52−60

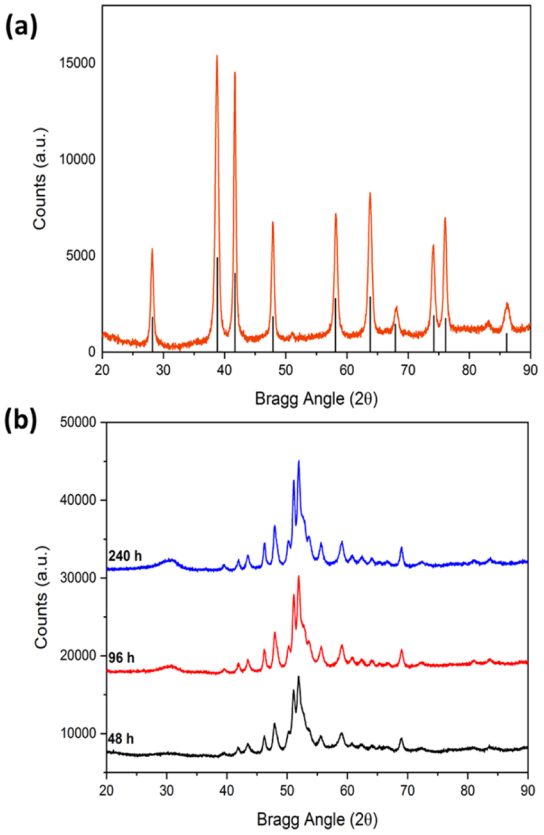

Figure 2. XRD diffractograms of (a) the hematite precatalyst and (b) the catalyst sample after exposure to CO hydrogenation conditions for 48 (black), 96 (red), and 240 h (blue) T-o-S. The black sticks in (a) are indicative of reflections corresponding to the α-Fe_2O_3 reference diffractogram from the Highscore Plus software package.

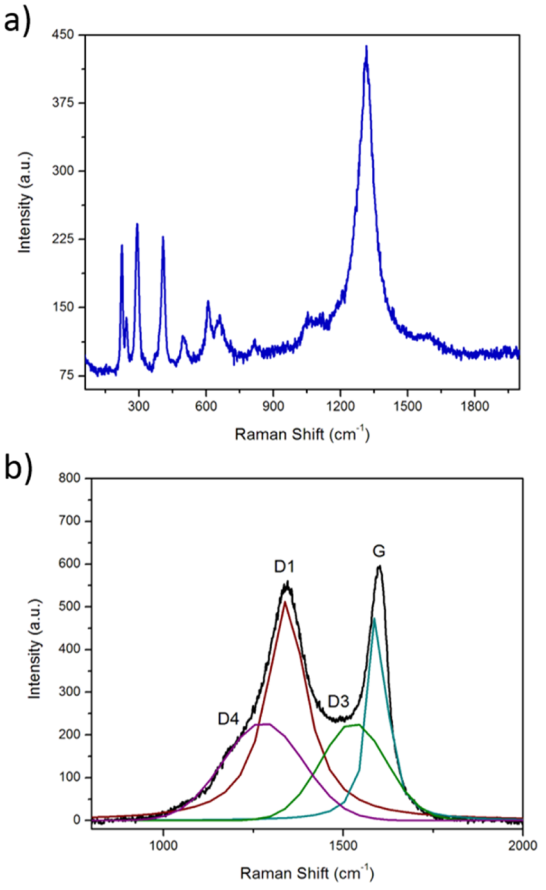

Figure 3. Raman spectra for the promoter-free iron oxide catalyst: (a) as-prepared and (b) LR-240 (exposure to CO hydrogenation conditions for 240 h). The colored lines (brown, green, purple, and turquoise), respectively, represent spectral deconvolution of carbonaceous D1, D3, D4, and G features (see the text).

catalysts and are assigned as follows: α-reactive carbon, β-amorphous carbon, and γ-bulk iron carbides.[17,18] From the profiles observed within this investigation using the large-scale reactor (Figure 4), only the β and γ features with respective peak maxima of ca. 630 and 680 K are observed for reaction times of 48, 96, and 240 h. The absence of the α peak (assigned as a precursor for the formation of the hydrocarbonaceous overlayer)[19] at these reaction times is considered further in Section 3.3. Quantification of the features in the TPO profiles of Figure 4 are tabulated in Table 2 and displayed in Figure 5.

Table 2 shows both the β and γ features to increase quite steeply up to ca. 100 h TOS; thereafter, the retention rate is retarded up to 240 h. Alongside the integrated TPO intensities for the 48, 96, and 240 h data sets, Figure 5 also includes intensity information taken from the earlier 0−24 h data set for CO hydrogenation over the same promoter-free catalyst under examination here.[18] It is noted that from 48 to 240 h, a different batch of catalyst was used. In this way, Figure 5 presents a more comprehensive perspective on the dependency of the α, β, and γ TPO features to reaction time using the large-scale INS reactor. The data set is normalized per gram of Fe in each case. Figure 5 shows that the amorphous carbon component (β) displays continued growth up to 96 h on stream, after which it saturates. The iron carbide component (γ) on the other hand exhibits an intense growth period up to 48 h on stream but, thereafter, shows a reduced rate of growth up to 240 h TOS. Overall, as a function of TOS utilizing the large-scale reactor, Figure 5 shows the following: (i) the α feature grows and then declines within the first 50 h, and (ii) the β and γ features progressively increase up to a region of 100−200 h, where their populations appear to saturate. The apparent "dip" at 50 h in the β profile of Figure 5 is thought to reflect some variance in the testing and/or post-reaction measurement of different batches of the hematite precatalyst.

Comparing the TPO profiles of Figure 5 with the XRD data of Figure 2 indicates that the previously adopted TPO assignments may be over-simplistic. Specifically, XRD unequivocally shows saturation of the iron carbide structure by 48 h T-o-S, yet the intensity of the γ feature in the TPO plots progressively increases significantly beyond that reaction time. Adding further uncertainty on the validity of the original assignments is the observation that the intensity profile of the TPO α species of Figure 5 more correctly correlates with the carbide feature detected by XRD (Figure 2). The matter of previously unrealized hidden complexity within the TPO spectrum will be revisited in the Discussion section (Section 4).

3.3. Inelastic Neutron Scattering. Figure 6 presents the INS spectra of the reacted samples and the sample that was dried and not exposed to reaction conditions (black), recorded at incident energies of 650 and 250 meV. The spectra for 3 and 6 h have previously been reported and are included here to convey the full hydrocarbonaceous overlayer evolution.[18] At

DOI: 10.1021/acs.iecr.9b04636
Ind. Eng. Chem. Res. 2020, 59, 52−60

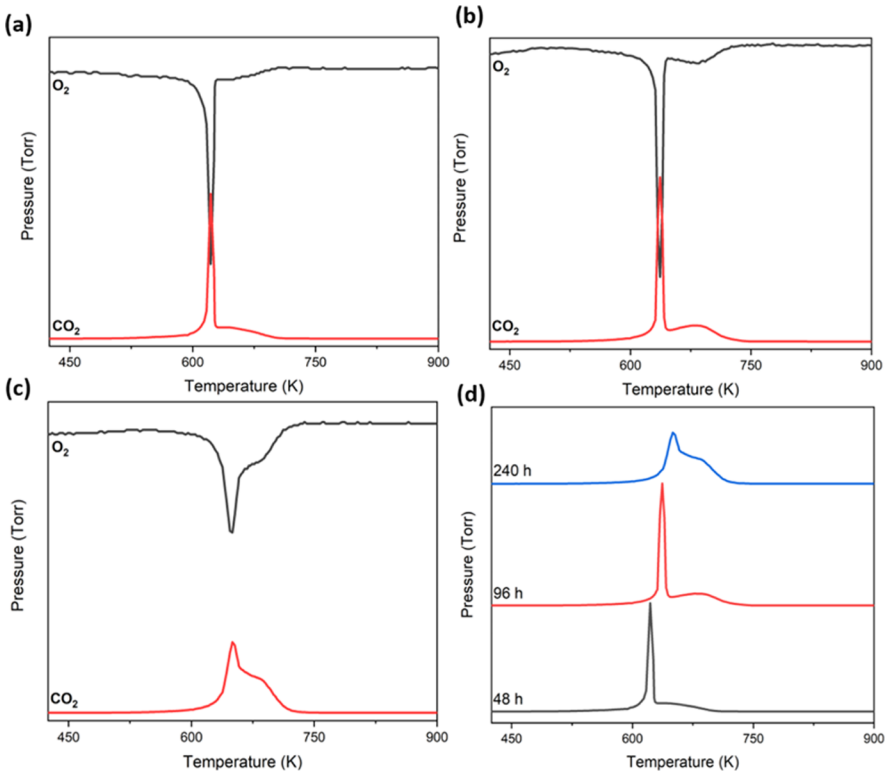

Figure 4. Ex situ TPO MS profiles with oxygen-associated consumption for samples exposed to CO hydrogenation conditions at 623 K for (a) 48 h, (b) 96 h, and (c) 240 h. (d) Stacked ex situ TPO MS profiles for 48 (black), 96 (red), and 240 h (blue) reactions.

Table 2. Quantified Peak Areas and Peak Maximum Temperatures from the TPO Studies Involving Samples from the Large-Scale INS Reactor

	β peak		γ peak	
sample	C content[b]	T_{max} [c]	C content[b]	T_{max} [c]
LR[a]-48	23.67	622	34.46	652
LR-96	48.74	636	34.00	682
LR-240	50.86	652	49.61	685

[a]LR-large-scale reactor. [b]C content in mmol C g_{Fe}^{-1}. [c]T_{max} in K.

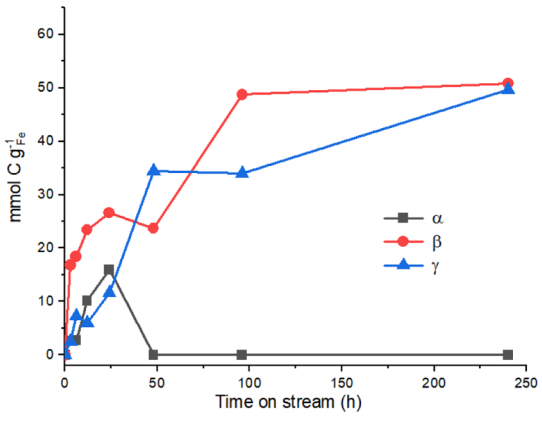

Figure 5. Carbon content of the three TPO species (α, β, γ) identified from TPO measurements, Figure 4 (see the text for assignments).

650 meV, Figure 6a shows that the spectra are defined by the presence of a ν(C−H) feature consisting of a main peak at 3048 cm^{-1} with a noticeable shoulder at ca. 2932 cm^{-1}. These bands are respectively assigned to the ν(C−H) modes of sp^2- and sp^3-hybridized carbons.[16,17] In contrast, the unreacted sample (0 h) is practically featureless, except for a small but noticeable peak at 3633 cm^{-1} that is attributed to the ν(O−H) mode of terminal hydroxyl groups. With T-o-S, the intensity of the ν(C−H) features increase, while the ν(O−H) mode is not present from 3 h onward, indicating a progressive deposition of the hydrocarbonaceous material and the removal of the small population of surface hydroxyls.

At 250 meV (Figure 6b), the clean, dehydrated sample has a significant peak at 797 cm^{-1}. Following previous studies, this can be attributed to a spinon mode of the hematite precatalyst.[17] The feature is no longer present at 3 h reaction time, signifying the loss of the hematite structure as the carburization process advances with extended T-o-S. The 3 h spectrum is characterized by the emergence of two weak features at 591 and 941 cm^{-1} that are, respectively, assigned to the A_{1g} Fe−O phonon mode of Fe_3O_4 and a combination of alkenic δ(C−H) and a possible magnetic interaction associated with Fe_3O_4.[17,31] At 6 h, there is an emergence of several other features which have all been described previously.[14−19] Briefly, they comprise a C−C torsion mode of edge carbon atoms contained within a polycyclic aromatic network (506 cm^{-1}),[32,33] out of plane C−H deformations of either an olefinic or aromatic group (807 and 871 cm^{-1}),[31,32] alkenic δ(C−H) (953 cm^{-1}),[14,16] and several aromatic δ(C−H) modes (1160, 1389, and 1451 cm^{-1}).[14−17] Evolution of each of these features is prominent up to 96 h, after which there is effectively little change in the spectral profile.

A significant advantage of using INS is the ability of the technique to determine the concentration of hydrogen within the analyzed samples.[34] Through previously established calibration procedures,[18,24] Figure 7 presents the degree of

DOI: 10.1021/acs.iecr.9b04636
Ind. Eng. Chem. Res. 2020, 59, 52−60

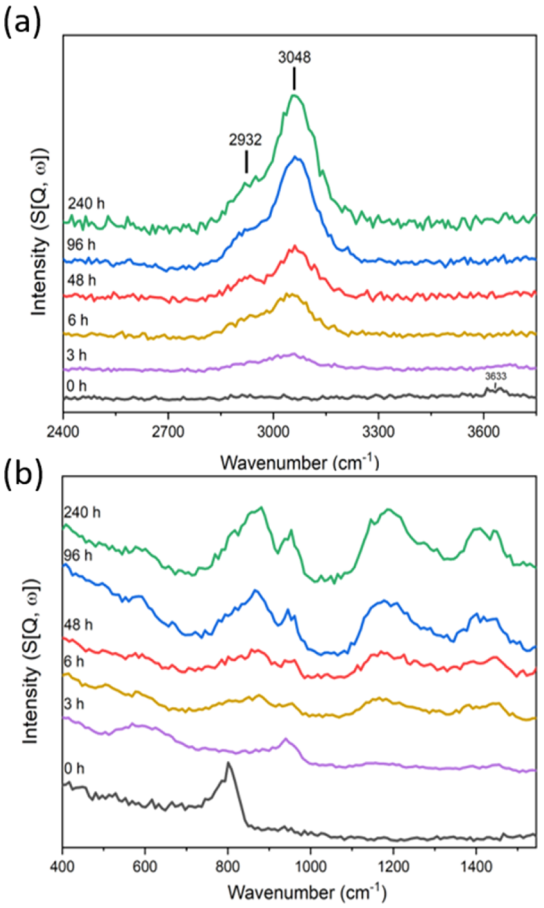

Figure 6. INS spectra for an Fe-based Fischer−Tropsch catalyst after continuous exposure to syngas (CO/H_2 = 1:2) at 623 K in the large-scale reactor for 0 (black), 3 (purple), 6 (yellow), 48 (red), 96 (blue), and 240 h (green): (a) incident energy = 650 meV and (b) incident energy = 250 meV.

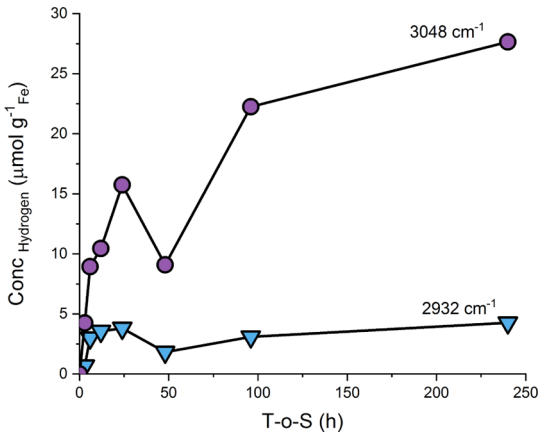

Figure 7. Hydrogen content (μmmol H g_{Fe}^{-1}) of the 2932 cm^{-1} (triangles) and 3048 cm^{-1} (circles) features identified in Figure 6. Data previously reported by Warringham et al. for the period 3−24 h are included in the figure[18] in order to convey the full evolutionary profile of the hydrocarbonaceous overlayer over a duration of 240 h.

hydrogen retention for the two resolved ν(C−H) modes. It is noted that Figure 7 is a combination of two sets of INS data from two separate batches of the same catalyst: 3−24 h on stream as previously reported by Warringham et al.[18] and 0, 48−240 h, as obtained from this investigation. Linking in with comments made in Section 3.2, as no characteristic features were observed in the MS profile at 48 h (Figure S1), the "dip" in intensity of the INS spectra at 48 h in Figure 7 is thought to reflect a degree of variance in the testing and post-reaction measurement of different batches of the hematite precatalyst rather than any structural dynamics of the catalyst. Moreover, repeat measurements of calibration standards on MAPS return an error of ±6.2%,[24] which is consistent with the generally continuous trends observed in these INS spectra of post-reaction catalysts.[15−18] Therefore, it is deduced that the anomalously low value for the 48 h sp^2-hybridized ν(C−H) mode in Figure 7 is reflective of some complication in that particular run. It is possible that this could be an unknown problem in the reaction testing procedure but, more likely, it could be due to poor alignment of the sample in the neutron beam. Nonetheless, with the exception of that one data point, Figure 7 essentially conveys a continuous profile.

Figure 7 is characterized by two distinct trends: first, the integrated intensity of the aliphatic ν(C−H) stretch at 2932 cm^{-1} saturates at approximately 24 h T-o-S; second, the sp^2-hybridized ν(C−H) stretch at 3048 cm^{-1}, representing olefinic and/or aromatic hydrocarbonaceous moieties, approaches saturation after 100−200 h T-o-S. This is important and new information, which indicates a degree of previously unrealized complexity in the evolutionary phase of the hydrocarbonaceous overlayer.

4. DISCUSSION

In order to better understand the INS profiles, it is first necessary to address the uncertainty connected with the original TPO assignments, as considered toward the end of Section 3.2. Concentrating first on the TPO α peak, this has been assigned to a carbonaceous species that is a precursor for the formation of the hydrocarbonaceous overlayer.[18] The coincidence of its intensity profile with that of the sp^3-hybridized ν(C−H) mode (Figure 7) more specifically links it to the aliphatic component of the overlayer. However, as exposed in Section 3.2, the TPO α peak could also be linked to iron carbide formation, as XRD (Figure 2b) shows iron carbide formation to have saturated over the period for which the TPO α peak is generated and consumed. One further possibility for the α feature is that part of its consumption could reflect this species additionally contributing to the growth of the TPO β and/or γ peaks for extended T-o-S (Figure 5), that is, in accordance with Niemantsverdriet's competition model;[18] the α feature could simultaneously be a precursor to the TPO β and/or γ features.

The possible assignment for the TPO γ peak is less convoluted than that discussed above for the α peak but, nonetheless, it necessarily requires revision. As noted in Section 3.2, it cannot exclusively be attributed to carbide formation. Given its profile (Figure 5) is broadly coincident that of the sp^2-hybridized ν(C−H) mode of the hydrocarbonaceous overlayer (Figure 7), an additional contribution of polyaromatic carbon is proposed.

These considerations indicate that the post-reaction TPO plots are more complicated than originally envisaged.[18] Indeed, it appears that certain peaks can be associated with various chemical transformations. Table 3 presents the revised assignments for the three TPO features connected with ambient pressure CO hydrogenation over an iron-based FTS catalyst at 623 K. Further analysis is clearly required to

DOI: 10.1021/acs.iecr.9b04636
Ind. Eng. Chem. Res. 2020, 59, 52−60

Table 3. Revised Probable Associations for the Three TPO Features Connected with Ambient Pressure CO Hydrogenation over an Unpromoted Iron-Based FTS Catalyst at 623 K

TPO peak	original assignment[18]	revised assignment
α	reactive carbon	(i) precursor to aliphatic component of the hydrocarbonaceous overlayer
		(ii) precursor to iron carbide formation
		(iii) precursor state to formation of the TPO β and/or γ features
β	amorphous carbon	amorphous carbon
γ	iron carbide	(i) iron carbide
		(ii) polyaromatic carbonaceous species

determine which of the proposed pathways the α component follows. This important matter constitutes "work in progress".

With an improved awareness of the TPO features presented in Figure 5, it is informative to concentrate on connections to the partitioning of hydrogen within the catalyst matrix as a function of T-o-S. Specifically, how does the temporal profile of the hydrocarbonaceous overlayer correspond to that observed for the reaction test data over this extended reaction coordinate? First, the CO hydrogenation test data in Figure 1 indicate the reaction system to be effectively operating in a steady-state regime from ca. 9 h. This is the benchmark time against which other temporal trends may be usefully compared. Interestingly, elemental analysis (Table 1) shows C and H values to continue to accrue way beyond that period, not achieving saturation values until 100−200 h T-o-S.

The XRD diffractograms (Figure 2) indicate the transition from hematite to Hägg carbide and a contribution from amorphous carbon; this is consistent with the Raman spectra presented in Figure 3. However, while the diffractograms show the extent of amorphous carbon to increase on increasing T-o-S, the intensity of the Hägg carbide features has saturated at 48 h. The maintenance of this structure over the period 48−240 h T-o-S connects with the stable reaction performance observed over this period (Section 3.1); a correlation supportive of the concept that Hägg carbide defines the active phase of a FTS catalyst.[8−11]

The intensity profile for the TPO β and γ features (Figure 5) broadly matches that observed for the sp^2-hybridized carbon ν(C−H) mode (Figure 7). This leads to the proposal that, over a period of up to ca. 200 h T-o-S, the amorphous carbon (β) and/or iron carbide and polyaromatic carbonaceous deposits (γ) evident in TPO measurements are responsible for the formation of the olefinic and/or aromatic component of the hydrocarbonaceous overlayer. If the α species is in fact a precursor to the β or γ as suggested above, then the α species is suggested to be the initial stage in a sequential pathway in the development of the hydrocarbonaceous overlayer, that is, α species → β and/or γ species → sp^2-hybridized ν(C−H) mode. This proposal is merely speculative at this stage. Nonetheless, each of the suggested pathways indicate the α species to have an integral role within the development of the evolving catalyst matrix. Indeed, these considerations illustrate the dynamic nature of the evolutionary phase of iron-based FTS catalysts undergoing CO hydrogenation at elevated temperatures and atmospheric pressure over extended periods of T-o-S.

Returning to the matter of catalytic performance, Table 4 contrasts the reaction times that correspond to completion of a particular component of the catalyst evolutionary process. Most notably, sustained catalytic turnover is attainable over short periods of time (≥9 h T-o-S), which can be loosely correlated with the formation of Hägg carbide features (≤48 h T-o-S). However, against this background, there is a progressive carburization process that leads to distinct profiles for specific entities detectable by TPO and INS. Indeed, modification of the carbonaceous and hydrocarbonaceous entities appears to undergo a relatively slow transitional phase that, seemingly, does not disturb catalyst performance. This slower modification of the catalyst matrix approaches completion over the period 100−200 h T-o-S. Collectively, this work shows that the journey from the hematite precatalyst to a stabilized material capable of supporting sustained syngas turnover is complex and involves a variety of molecular entities, that is, iron oxides, iron carbides, carbonaceous entities, and a hydrocarbonaceous overlayer.

Table 4. Values of T-o-S That Correspond to Completion of a Particular Component of the Catalyst Evolutionary Process as Determined by (a) Reaction Testing, (b) Elemental Analysis, (c) XRD, (d) TPO, and (e) INS

technique	component of the catalyst evolutionary process	T-o-S corresponding to completion of a particular component of the catalyst evolutionary process/h
reaction testing	steady-state operation in CO hydrogenation test reaction	∼9
elemental analysis	(i) carbon	100−200
	(ii) hydrogen	100−200
powder XRD	Hägg carbide	≤48
TPO	(i) α peak	∼50
	(ii) β and γ peaks	100−200
INS	(i) ν(C−H) sp^3-hybridized carbon	∼24
	(ii) ν(C−H) sp^2-hybridized carbon	100−200

5. CONCLUSIONS

Ambient pressure CO hydrogenation over a promoter-free hematite catalyst at 623 K has been investigated for extended periods of T-o-S of up to 10 days (240 h) utilizing approximately 10 g of catalyst charge. Characterization of the catalyst through INS, elemental analysis, TPO, XRD, and Raman spectroscopy leads to the following conclusions:

- Post-reaction ex situ XRD indicates only the Hägg carbide to be present within the bulk catalyst from 48 h onward.
- For reaction times ≥48 h, TPO measurements show only amorphous carbon (peak β) and iron carbide and polyaromatic carbonaceous species (peak γ) to be present. The reactive carbonaceous species (peak α) grows and decays to ultimately zero concentration over the period 0−48 h T-o-S.
- INS analysis of the reacted catalyst samples identifies the presence of sp^2- and sp^3-hybridized C−H species, with quantification of the ν(C−H) modes indicating the concentration of aliphatic C−H species to saturate after

DOI: 10.1021/acs.iecr.9b04636
Ind. Eng. Chem. Res. 2020, 59, 52−60

approximately 24 h T-o-S. In contrast, the concentration of olefinic/aromatic C−H entities progressively increase up to ∼200 h before appearing to reach saturation.

- The development of the amorphous carbon (β) and iron carbide + polyaromatic carbonaceous (γ) entities that occurs over a catalyst conditioning period of ca. 200 h correlate with the formation of the olefinic and/or aromatic component of the hydrocarbonaceous overlayer.
- The TPO α species is suggested to play an integral part in the catalyst evolutionary process and may be associated with the following three pathways: (i) a precursor to iron carbide formation; (ii) a precursor to the formation of the aliphatic component of the hydrocarbonaceous overlayer; and (iii) a precursor to either the β or γ TPO features.
- From inspection of TPO and INS intensity profiles, it is concluded that under the stated reaction conditions, the overall catalyst evolutionary phase requires approximately 200 h T-o-S to achieve completion.
- Steady-state operation of the catalytic system is not directly coupled to the TPO β and γ entities, nor is it connected to the development of the olefinic/aromatic component of the hydrocarbonaceous overlayer.

■ ASSOCIATED CONTENT

Supporting Information

The Supporting Information is available free of charge at https://pubs.acs.org/doi/10.1021/acs.iecr.9b04636.

Full reaction profile for the sample exposed to CO hydrogenation conditions at 623 K for 96 h; powder XRD with Rietveld refinement of the calcined hematite catalyst before exposure to reaction conditions; Rietveld refinement of the hematite catalyst after exposure to ambient pressure CO hydrogenation at 623 K for 24, 96, and 240 h T-o-S (PDF)

■ AUTHOR INFORMATION

Corresponding Authors

*Email: pbw@st-andrews.ac.uk (P.B.W.).
*E-mail: David.Lennon@glasgow.ac.uk. Phone: +44-141-330-4372 (D.L.).

ORCID

Paul B. Webb: 0000-0003-2532-344X
Stewart F. Parker: 0000-0002-3228-2570
David Lennon: 0000-0001-8397-0528

Notes

The authors declare no competing financial interest.

■ ACKNOWLEDGMENTS

Sasol Ltd., the EPSRC (award reference EP/P505534/1), and the University of Glasgow are thanked for the provision of a postgraduate studentship (ALD). The STFC Rutherford Appleton Laboratory is thanked for access to neutron beam facilities. The Royal Society is thanked for the provision of an Industry Fellowship (PBW). Professor Bob Tooze (Drochaid Research Services, St. Andrews, UK) is thanked for helpful discussions. Dr Giovanni Rossi and Dr James Campbell (School of Chemistry, University of Glasgow) are thanked for assistance with the neutron measurements.

■ REFERENCES

(1) De Smit, E.; Weckhuysen, B. M. The Renaissance of Iron-Based Fischer-Tropsch Synthesis: on the Multifaceted Catalyst Deactivation Behaviour. *Chem. Soc. Rev.* **2008**, *37*, 2758−2781.

(2) Steynberg, A. P. Introduction to Fischer Tropsch Technology. *Studies in Surface Science and Catalysis*; Elsevier, 2004;Vol. *152*, pp 1−63.

(3) Van de Loosdrecht, J.; Botes, F. G.; Ciobica, I. M.; Ferreira, A.; Gibson, P.; Moodley, D. J.; Saib, A. M.; Visage, J. L.; Weststrate, C. J.; Niemantsverdriet, J. W. Fischer-Tropsch Synthesis: Catalysts and Chemistry. *Comprehensive Inorganic Chemistry II*; Eslvier: Oxford, 2013; Vol. *7*, pp 525−557.

(4) Ning, W.; Koizumi, N.; Chang, H.; Mochizuki, T.; Itoh, T.; Yamada, M. Phase transformation of unpromoted and promoted Fe catalysts and the formation of carbonaceous compounds during Fischer-Tropsch synthesis reaction. *Appl. Catal., A* **2006**, *312*, 35−44.

(5) de Smit, E.; Cinquini, F.; Beale, A. M.; Safonova, O. V.; van Beek, W.; Sautet, P.; Weckhuysen, B. M. Stability and Reactivity of ε-χ-θ Iron Carbide Catalyst Phases in Fischer-Tropsch Synthesis: Controlling μc. *J. Am. Chem. Soc.* **2010**, *132*, 14928−14941.

(6) Niemantsverdriet, J. W.; Van der Kraan, A. M.; Van Dijk, W. L.; Van der Baan, H. S. Behaviour of Metallic Iron Catalysts during Fischer-Tropsch Synthesis Studied with Mössbauer Spectroscopy, X-ray Diffraction, Carbon Content Determination, and Reaction Kinetic Measurements. *J. Phys. Chem.* **1980**, *84*, 3363−3370.

(7) Dry, M. E. *The Fischer-Tropsch Synthesis, Catalysis: Science and Technology*; Springer-Verlag: New York, 1981; pp 160−255.

(8) Gracia, J. M.; Prinsloo, F. F.; Niemantsverdriet, J. W. Mars-van Krevelen-like mechanism of CO hydrogenation on an iron carbide surface. *Catal. Lett.* **2009**, *133*, 257−261.

(9) Shroff, M. D.; Kalakkad, D. S.; Coulter, K. E.; Kohler, S. D.; Harrington, M. S.; Jackson, N. B.; Sault, A. G.; Datye, A. K. Activation of Precipitated Iron Fischer-Tropsch Synthesis Catalysts. *J. Catal.* **1995**, *156*, 185−207.

(10) Li, S.; Ding, W.; Meitzner, G. D.; Iglesia, E. Spectroscopic and transient kinetic studies of site requirements in iron-catalyzed Fischer-Tropsch synthesis. *J. Phys. Chem. B* **2002**, *106*, 85−91.

(11) Zhang, J.; Abbas, M.; Chen, J. The evolution of Fe phases of a fused iron catalyst during reduction and Fischer-Tropsch synthesis. *Catal. Sci. Technol.* **2017**, *7*, 3626−3636.

(12) Pérez-Alonso, F. J.; Herranz, T.; Rojas, S.; Ojeda, M.; Lopez Granados, M.; Terreros, P.; Fierro, J. L. G.; Gracia, M.; Gancedo, J. R. Evolution of the bulk structure and surface species on Fe-Ce catalysts during the Fischer-Tropsch synthesis. *Green Chem.* **2007**, *9*, 663−670.

(13) Buker, D. M.; Nowicki, L.; Patel, S. A. Activation studies with an iron Fischer-Tropsch catalyst in Fixed bed and stirred tank slurry reactors. *Can. J. Chem. Eng.* **1996**, *74*, 399−404.

(14) Hamilton, N. G.; Silverwood, I. P.; Warringham, R.; Kapitán, J.; Hecht, L.; Webb, P. B.; Tooze, R. P.; Parker, S. F.; Lennon, D. Vibrational Analysis of an Industrial Fe-based Fischer-Tropsch Catalyst Employing Inelastic Neutron Scattering. *Angew. Chem., Int. Ed.* **2013**, *52*, 5608−5611.

(15) Hamilton, N. G.; Warringham, R.; Silverwood, I. P.; Kapitán, J.; Hecht, L.; Webb, P. B.; Tooze, R. P.; Zhou, W.; Frost, C. D.; Parker, S. F.; Lennon, D. The Application of Inelastic Neutron Scattering to Investigate CO hydrogenation over an Iron Fischer-Tropsch Synthesis Catalyst. *J. Catal.* **2014**, *312*, 221−231.

(16) Warringham, R.; Hamilton, N. G.; Silverwood, I. P.; How, C.; Webb, P. B.; Tooze, R. P.; Zhou, W.; Frost, C. D.; Parker, S. F.; Lennon, D. The Application of Inelastic Neutron Scattering to Investigate a Hydrogen Pre-treatment Stage of an Iron Fischer-Tropsch Catalyst. *Appl. Catal., A* **2015**, *489*, 209−217.

(17) Warringham, R.; McFarlane, A. R.; MacLaren, D. A.; Webb, P. B.; Tooze, R. P.; Taylor, J.; Ewings, R. A.; Parker, S. F.; Lennon, D. The Application of Inelastic Neutron Scattering to Explore the Significance of a Magnetic Transition in an Iron-Based Fischer-Tropsch Catalyst that is Active for the Hydrogenation of CO. *J. Chem. Phys.* **2015**, *143*, 174703.

DOI: 10.1021/acs.iecr.9b04636
Ind. Eng. Chem. Res. 2020, 59, 52−60

(18) Warringham, R.; Davidson, A. L.; Webb, P. B.; Tooze, R. P.; Ewings, R. A.; Parker, S. F.; Lennon, D. Examining the temporal behaviour of the hydrocarbonaceous overlayer on an iron based Fischer-Tropsch catalyst. *RSC Adv.* **2019**, *9*, 2608−2617.
(19) Warringham, R.; Davidson, A. L.; Webb, P. B.; Tooze, R. P.; Parker, S. F.; Lennon, D. Perspectives on the effect of sulfur on the hydrocabronacous overlayer on iron Fischer-Tropsch catalysts. *Catal. Today* **2020**, *339*, 32−39.
(20) Borodziński, A.; Cybulski, A. The kinetic model of hydrogenation of acetylene-ethylene mixtures over palladium surface covered by carbonaceous deposits. *Appl. Catal., A* **2000**, *198*, 51−66.
(21) Warringham, R.; Bellaire, D.; Parker, S. F.; Taylor, J.; Ewings, R. A.; Goodway, C. M.; Kibble, M.; Wakefield, S. R.; Jura, M.; Dudman, M. P.; Tooze, R. P.; Webb, P. B.; Lennon, D. Sample environment issues relevant to the acquisition of inelastic neutron scattering measurements of heterogeneous catalyst samples. *J. Phys.: Conf. Ser.* **2014**, *554*, 012005.
(22) Mitchell, P. C. H.; Parker, S. F.; Ramirez-Cuesta, A. J.; Tomkinson, J. *Vibrational Spectroscopy Using Neutrons with Application in Chemistry, Biology, Material Science and Catalysis. Series on Neutron Techniques and Applications*; World Scientific: Singapore, 2005; Vol. 3.
(23) Parker, S. F.; Lennon, D.; Albers, P. W. Vibrational Spectroscopy with Neutrons: A Review of New Directions. *Appl. Spectrosc.* **2011**, *65*, 1325−1341.
(24) Silverwood, I. P.; Hamilton, N. G.; Laycock, C. J.; Staniforth, J. Z.; Ormerod, R. M.; Frost, C. D.; Parker, S. F.; Lennon, D. Quantification of Surface Species Present on a Nickel/Alumina Methane Reforming Catalyst. *Phys. Chem. Chem. Phys.* **2010**, *12*, 3102−3107.
(25) Shroff, M. D.; Datye, A. K. The importance of passivation in the study of iron Fischer-Tropsch catalysts. *Catal. Lett.* **1996**, *37*, 101−106.
(26) Silverwood, I. P.; Hamilton, N. G.; McFarlane, A. R.; Kapitán, J.; Hecht, L.; Norris, E. L.; Mark Ormerod, R.; Frost, C. D.; Parker, S. F.; Lennon, D. Application of Inelastic Neutron Scattering to Studies of CO2 Reforming of Methane Over Alumina-Supported Nickel and Gold-Doped Nickel Catalysts. *Phys. Chem. Chem. Phys.* **2012**, *14*, 15214−15225.
(27) Galvis, H. M. T.; Koeken, A. C. J.; Bitter, J. H.; Davidian, T.; Ruitenbeek, M.; Dugulan, A. I.; de Jong, K. P. Effect of sodium and sulfur on catalytic performance of supported iron catalysts for the Fischer-Tropsch synthesis of lower olefins. *J. Catal.* **2013**, *303*, 22−30.
(28) Tuinstra, F.; Koenig, J. L. Raman spectrum of graphite. *J. Chem. Phys.* **1970**, *53*, 1126−1130.
(29) Pimenta, M. A.; Dresselhaus, G.; Dresselhaus, M. S.; Cançado, L. G.; Jorio, A.; Saito, R. Studying disorder in graphite-based systems by Raman spectroscopy. *Phys. Chem. Chem. Phys.* **2007**, *9*, 1276−1290.
(30) Sadezky, A.; Muckenhuber, H.; Grothe, H.; Niessner, R.; Pöschl, U. Raman microspectroscopy of soot and related carbonaceous materials: Spectral analysis and structural information. *Carbon* **2005**, *43*, 1731−1742.
(31) Chamritski, I.; Burns, G. Infrared- and Raman-Active Phonons of Magnetite, Maghemite, and Hematite: A Computer Simulation and Spectroscopic Study. *J. Phys. Chem. B* **2005**, *109*, 4965−4968.
(32) Lin-Vein, D.; Colthup, N. B.; Fateley, W. G.; Graselli, J. G. *The Handbook of Infrared and Raman Characteristic Frequencies of Organic Molecules*; Academic Press: Boston, 1991.
(33) Albers, P. W.; Pietsch, J.; Krauter, J.; Parker, S. F. Investigations of Activated Carbon Catalyst Supports from Different Natural Sources. *Phys. Chem. Chem. Phys.* **2003**, *5*, 1941−1949.
(34) Albers, P. W.; Lennon, D.; Parker, S. F., Catalysis. *Neutron Scattering: Applications in Biology, Chemistry, and Materials Science*; Elsevier, 2017; Vol. *49*, pp 279−348.

DOI: 10.1021/acs.iecr.9b04636
Ind. Eng. Chem. Res. 2020, 59, 52−60